

Scalable fabrication of MnO₂ nanostructure deposited on free-standing Ni nanocone arrays for ultrathin, flexible, high-performance micro-supercapacitor†

Cite this: DOI: 10.1039/c4ee01195c

Zijin Su,^a Cheng Yang,^{*a} Binghe Xie,^a Ziyin Lin,^b Zhexu Zhang,^a Jingping Liu,^a Baohua Li,^a Feiyu Kang^{ac} and Ching Ping Wong^b

Ultrathin and flexible power sources are essential for the rapid development of portable and wearable electronics. The deployment of 3-dimensional (3-D) nanostructured materials on the current collectors has recently emerged as a promising strategy for preparing high-performance supercapacitors. Additionally, it is equally important to develop an appropriate device packaging technique, so as to maximize the improvement of the electrode performance characteristic. Herein, we develop a simple and efficient method for fabricating ultrathin and flexible supercapacitor electrodes containing a manganese dioxide (MnO₂) nanostructure deposited onto 3-D nickel nanocone arrays (NCAs). The MnO₂-NCAs electrode was prepared by an electro-deposition technology, which involves the cathode deposition of NCAs on a titanium carrier film as the current collector and subsequent anode deposited from the MnO₂ nanostructures as the active material. The electrode can be peeled off from the carrier film and thus the resulting freestanding electrode is as thin as 3 μm, and exhibits outstanding mechanical robustness, high specific capacitance (632 F g⁻¹), enhanced energy density (52.2 W h kg⁻¹) and excellent cycle performance (95.3% retention after 20 000 cycles). We further fabricated ultrathin supercapacitors with a total thickness of ~27 μm, which achieved unprecedented features including superior energy density by volume (2.7 × 10⁻³ W h cm⁻³), superior flexibility and reliability. We demonstrated the application of the MnO₂-NCAs supercapacitor as an ultrathin power source such as driving a LED indicator. This technology may find vast applications in future wearable electronics.

Received 16th April 2014

Accepted 28th May 2014

DOI: 10.1039/c4ee01195c

www.rsc.org/ees

Broader context

With the growing demand for portable and wearable electronic devices, it is imperative to develop ultrathin, flexible and high-performance energy storage systems. Therefore, the related scalable preparation technique of ultrathin electrodes is more important than ever. The current manuscript reports the design and fabrication of 3-D hierarchical structured MnO₂/Ni nanocone arrays as the electrode, which is as thin as 3 μm and can be peeled off from the metal carrier substrate. A supercapacitor device based on this new material can reach a maximum energy density of 2.7 × 10⁻³ W h cm⁻³ and maintain less than 10% capacity fading after 5000 cycles. Based on a roll-to-roll process, a 1.3 m electrode was fabricated. This technique may have an immediate impact on the development of micro-power modules and flexible electronics.

Introduction

Ultrathin, flexible and high-performance energy storage devices are essential for the development of portable and wearable consumer electronics. Especially, thin film supercapacitors are expected to play an important role in applications of *e.g.* implantable biosensors, active tags, and micro-electromechanical systems (MEMS).¹ Compared to the other thin film secondary energy storage devices *e.g.* lithium ion batteries, the thin film supercapacitor exhibits a series of advantages, such as faster charge/discharge rates (within several seconds), much longer lifetimes (more than 1 000 000 cycles) and higher power density, which renders it very

^aDivision of Energy and Environment, Graduate School at Shenzhen, Tsinghua University, Shenzhen 518055, China. E-mail: yang.cheng@sz.tsinghua.edu.cn

^bSchool of Materials Science and Engineering, Georgia Institute of Technology, 771 Ferst Dr., Atlanta, GA 30332, USA

^cState Key Laboratory of New Ceramics and Fine Processing, Department of Materials Science and Engineering, Tsinghua University, Beijing 100084, China

† Electronic supplementary information (ESI) available: XRD, SEM, TEM, XPS, electrochemical property of electrode materials and asymmetric supercapacitors, and details of the electrode fabricated by roll-to-roll process are elucidated. Two movies showing the roll-to-roll process and the flexible test of as-prepare supercapacitor respectively are also included. See DOI: 10.1039/c4ee01195c

promising for complementing or replacing batteries and electrolytic capacitors.² In spite of its great importance, there still remain challenges to make ultrathin and high-performance supercapacitors in a convenient and efficient way, due to process complexity. Recently, micro-supercapacitors were made using carbon nanomaterials, *e.g.* graphene, carbon nanotubes, onion-like carbon, *etc.*^{3–5} However, the specific capacitance is usually less than 200 F g^{-1} , and the volumetric energy density is lower than $2 \times 10^{-3} \text{ W h cm}^{-3}$;³ such low performance is related to the low electrical double layer capacitance at carbon–electrolyte interfaces. Moreover, the mechanical properties (such as peeling strength) of the nanoporous carbon electrodes are usually quite poor, which hinders their applications in harsh conditions.

In order to improve the capacitance, pseudocapacitive materials can be used as electrode materials including RuO_2 ,^{6,7} MnO_2 ,^{8–10} Co_3O_4 ,^{11,12} and NiO ,¹³ *etc.* Excellent specific capacitance was achieved in conventional bulk supercapacitors for these materials.^{14,15} However, their performance characteristics in thin-film devices have been unsatisfactory;^{16,17} this is because the fabrication of thin devices is very complex and usually has less controllability on the crystalline phase and morphology of pseudocapacitive materials which are critical for the material performance. As a result, the use of pseudocapacitive materials in ultrathin flexible microcapacitors is very limited.

Among various transition-metal oxides, MnO_2 has been considered as one of the most promising materials due to its environmental friendliness, low cost and high theoretical specific capacitance (1370 F g^{-1}).¹⁸ However, the poor electrical conductivity of MnO_2 (10^{-5} – $10^{-6} \text{ S cm}^{-1}$) is an obstacle for its application in energy storage.¹⁹ An effective way to improve electrical conductivity and to boost electrochemical performance is to conformally deposit MnO_2 onto highly conductive and well-ordered micro-/nanostructures, which serve as both a current collector and mechanical support with greatly enhanced ionic transport. For example, literature sources have reported the deposition of MnO_2 on 1-D high aspect ratio nanowire/nanotube arrays and 3-D carbon materials.^{20–23} However, the mechanical properties of the substrate are often problematic. For example, arrays with a high aspect ratio collapse towards the neighbors, leading to decrease of the useful surface and limited accessibility to the electrolyte. Another important consideration for such a device is the good adhesion between MnO_2 and the substrate, so that the active material can resist mechanical impact and abrasion.^{9,24}

Most recently, there have been significant advances regarding the technology of micro-supercapacitors. Jayan Thomas *et al.* reported a spin-on nanoprint method to print large-area and well-ordered nanostructured supercapacitor electrodes.²³ They deposited MnO_2 on the surface of polyacrylonitrile nanopillars with a sputtered Au–Pd layer. The as-prepared supercapacitor electrodes showed high specific capacitance (603 F g^{-1}) and enhanced energy density ($50.68 \text{ W h kg}^{-1}$), which was benefited by effective exploitation of MnO_2 with less structure collapse. Su Zijin *et al.* recently reported the co-electro-deposition of MnO_2 /PEDOT:PSS onto a stainless steel mesh for high areal capacitance supercapacitor

electrodes, which showed high mechanical strength for resisting tape peeling and the total thickness of the electrode was as thin as $70 \mu\text{m}$.⁹ El-Kady *et al.* reported high-performance laser scribed graphene for flexible microsupercapacitors using a graphene electrode ($7.6 \mu\text{m}$ in thickness) with an in-plane structure.⁴ There is general expectation for further advances of the micro-supercapacitor technology with features such as lower materials cost, higher throughput of preparation, and even thinner and better mechanical strength of the electrode. In this way, there is an urgent need to develop convenient, low-cost and scalable techniques for preparing ultrathin, flexible, nanostructured electrodes for micro-supercapacitors.

Here, we prepared highly ordered ultrathin Ni nanocore arrays (NCAs) by a one-step electro-deposition (cathode-deposition) method on the surface of a Ti plate (Fig. 1).²⁵ The formation of NCAs is through screw dislocation growth on a defective crystal surface.²⁶ NCAs were used as the support of silicon for the anode in lithium ion batteries due to the high aspect ratio, excellent electrical conductivity and structure stability;²⁷ yet there are no scientific reports available regarding their use for supercapacitor fabrications.

For the first time, we demonstrated that NCAs electro-deposited with MnO_2 nanostructure (MNN) could be peeled off from the carrier substrate (Ti film) and be used as the free-standing, ultrathin, and flexible supercapacitor electrode for energy storage applications. Since both NCAs and MnO_2 nanostructures are prepared through an electro-deposition process, our method is very simple, easily controllable, and scalable. As the height of the NCAs is less than $2 \mu\text{m}$, and the whole thickness of the electrode is as thin as about $3 \mu\text{m}$, which is thinner than the laser-scribed graphene electrode ($7.6 \mu\text{m}$);⁴ the electrodes prepared in this way is suitable for ultrathin energy storage device applications. This thickness is even smaller than commercial Cu and Al foils for making soft-packed batteries. As compared with transition metal oxides synthesized by conventional methods (*e.g.* sol–gel²⁸ and hydrothermal ones^{11,29}), the capacitance of our MNN is quite stable and remains 95.3% of the initial value after 20 000 cycles. Taking this technical breakthrough, the whole thickness of the as-fabricated supercapacitor is only as small as $27 \mu\text{m}$. The capacitance of the MNN electrode is as high as 632 F g^{-1} which is higher than some recently reported graphene-based supercapacitors (graphene/CNTs³⁰ and graphene/ MnO_2 (ref. 31–33)) and the highest energy density can be 52.2 W h kg^{-1} with a power density of 2.0 kW kg^{-1} . Even the mass loading of MnO_2 reaches 0.38 mg cm^{-2} , the specific capacitance can be as high as 227 F g^{-1} (Fig. S12†). Flexible asymmetric supercapacitors with outstanding electrochemical performance were fabricated using MNN and activated carbon (AC) as a counter electrode. In our previous work,⁹ we reported that the potential window of the MnO_2 /AC asymmetric supercapacitor with Na_2SO_4 aqueous electrolyte can be as high as 2.0 V . In order to improve the energy density of the flexible microsupercapacitor, ionic liquid gel electrolyte (also called ionogel³⁴) was used to allow the operation of the device at a voltage window of 2.5 V . It demonstrates extremely high flexibility and can be bent at different angles without an apparent change in electrochemical performance. Additionally,

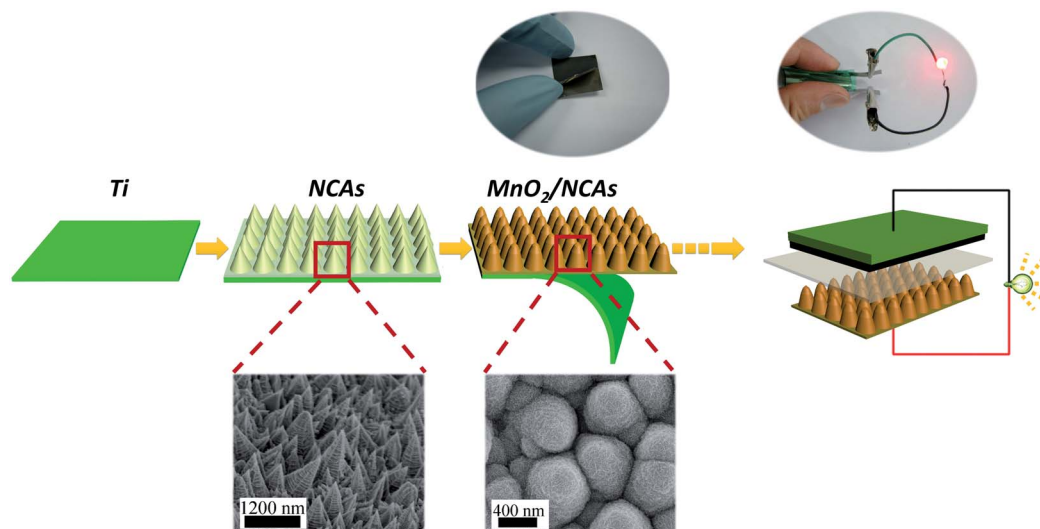


Fig. 1 Schematic illustration of the fabrication process for an ultrathin supercapacitor. The highly ordered NCAs were vertically grown on the Ti substrate. MnO_2 was then deposited onto the surface of Ni nanocones for a high-performance supercapacitor electrode. The Ni nanocone-based MnO_2 electrode which is as thin as $3 \mu\text{m}$ can be peeled off from Ti substrate. AC was used as the counter electrode and ionogel electrolyte was used for the ultrathin all-solid-state micro-supercapacitor.

the process of electrode preparation can be completed on a roll-to-roll instrument for scalable fabrication. A 1.3 m electrode has been provided for demonstration (Fig. 4d and S19[†]).

Experimental

Synthesis of NCAs

The NCAs were fabricated by an electro-deposition method. A commercial Ni plate (99.9%) was employed as the anodic electrode and NCAs were deposited on a Ti plate cathode. The Ti and Ni plates were washed by ultrasonication in a mixed solution of acetone and ethanol (1 : 1 vol) for more than an hour. All the solutions in the experiments were prepared with chemicals of analytical grade and deionized water. The electro-deposition solution was composed of 0.84 M $\text{NiCl}_2 \cdot 6\text{H}_2\text{O}$ (providing Ni ions), 0.75 M NH_4Cl (crystal modifier) and 1.00 M H_3BO_3 (pH buffer). The solution was kept at a temperature of 60°C and a pH of 4.0. 10 wt% HCl and 10 wt% NaOH were used to adjust the pH value of the electrolyte solution. The electro-deposition process was carried out at a current density of 20 mA cm^{-2} for 8 min. After the deposition process, the samples were thoroughly rinsed with deionized water and dried in air. The preparation of NCAs can be scaled up by the as-design roll-to-roll device, as shown in Fig. S19[†]. The Ti bar was cut as wide as 2.0 cm and wound by two rollers. The deposition process can be controlled by an electric motor integrated in the roll-to-roll device.

Preparation of NCAs supported MnO_2 electrodes and AC electrodes

The electrodes were fabricated by an anode deposition method. NCAs were used as anode and the counter electrode was a platinum plate. The deposition process was conducted in a 0.05 M $\text{Mn}(\text{Ac})_2$ aqueous solution with a 3.0 V DC voltage. MnO_2

deposited on a Ni plate (MNP) was used as the control sample. The as-prepared electrode was rinsed with deionized water several times to remove impurities and dried at 60°C for 1 hour. The mass loading of MnO_2 was calculated by weighting the electrodes before and after MnO_2 deposition. NCAs supported MnO_2 electrode was then peeled off from the Ti plate. The deposition of MnO_2 can also be scaled up by the as-design roll-to-roll process. The anode was a Ti bar with NCAs deposition.

Fabrication of ion liquid gel electrolyte

An ionogel electrolyte was prepared by mixing together 1-ethyl-3-methylimidazolium tetrafluoroborate (EMIMBF_4) with fumed silica (FS) nanopowder (1 ml EMIMBF_4 /400 mg FS). This mixture was stirred in a glove box under an Ar atmosphere for more than 5 hours to get a clear viscous ionogel (FS-IL) for asymmetric supercapacitor devices.

Materials characterization and electrochemical measurements

The morphology and microstructure were characterized by field emission scanning electron microscopy (FE-SEM, HITACH S4800, Japan) and transmission electron microscopy TEM, FEI G2 spirit. Measurements (ESCALAB 250Xi) were performed to analyze the surface species and their chemical states. The deconvolution and spectral line fitting were carried out using XPS Peak 4.0. The phase analysis was conducted on X-ray diffraction measurements (XRD, BrukerDS RINT2000/PC). The mechanical properties were tested by an electromechanical universal testing machine (MTS, CMT6104).

Cyclic voltammetry (CV), galvanostatic charging/discharging (GCD) and electrochemical impedance spectroscopy (EIS) of the as-prepared samples were investigated on an electrochemical station (VMP3, Bio-Logic, France) by a three-electrode configuration in a Na_2SO_4 (0.5 M) aqueous electrolyte. Platinum and

saturated calomel electrode (SCE) were used as counter and reference electrodes, respectively. The applied potential window of CV and GCD was in the range from 0 V to 0.8 V. The EIS was conducted in the frequency range between 100 KHz and 0.01 Hz with an amplitude of 5 mV at an open-circuit potential. The specific capacitance was calculated from the CVs and discharging curves according to the equations:

$$C = \frac{1}{m \cdot \nu \cdot \Delta V} \int i(V) dV \quad (1)$$

$$C = \frac{I \cdot \Delta t}{m \Delta U} \quad (2)$$

where C is the specific capacitance of the materials, m is the MnO_2 mass loading on the substrate which was determined by the different weight of the Ni nanocone electrode before and after MnO_2 deposition, ν is the scan rate, ΔV is the potential window in the CV curves, $i(V)$ is the voltammetric current, I is the applied current, ΔU is the potential window in the discharging process and Δt is the discharging time.³⁵ The energy and power density (E and P) were calculated by the equation:

$$E = \int IV(t) dt / (\text{Vol}) \quad (3)$$

$$P = E / \Delta t \quad (4)$$

where I is the discharging current, $V(t)$ is the voltage, dt is the time differential, Δt is the discharging time and Vol refers to the volume of the device, respectively. It is worth mentioning that the volumetric capacitance includes active material, the substrate (or the current collector) and the separator with electrolyte.

Results and discussion

Fig. 1 illustrates the fabrication process of the ultrathin and flexible supercapacitor. Vertical Ni nanocones were grown on the Ti substrate as the current collector of the supercapacitor. A MnO_2 nanostructure was then deposited onto the surface of NCAs and acted as the active material. The excellent adhesion between the MnO_2 layer and Ni nanocone substrate renders the electrode free of binder or conductive additive. The NCAs thin film can be easily peeled off from the Ti substrate, and a free-standing MNN electrode (as thin as 3 μm) was obtained. The reason for the easy off-peeling from the Ti substrate may be related to the weak interaction between Ni and the surface oxide layer of commercial Ti foil. In order to improve the operating voltage of the all-solid-state supercapacitor, activated carbon (AC) was used as a counter electrode and EMIMBF₄/FS ionogel was used as an electrolyte. EMIMBF₄ ion liquid has been successfully used as the supercapacitor electrolyte due to its wide working potential.^{36,37} The supercapacitor has a high flexibility and can light up a red LED under a bending state.

The morphology of NCAs is shown in Fig 2a, which suggests that most nanocones grow along the direction vertical to the substrate. The average height of the Ni nanocones was estimated to be about 1.2 μm from the SEM images. The apex

angles of all nanocones are $\sim 30^\circ$. The surface of the cones is rough, which is beneficial for the good adhesion between deposited MnO_2 and the current collector. The surface area of the NCAs is estimated to be 3.25 times that of the planar Ni substrate (Scheme 1, ESI†). X-ray diffraction (XRD) analysis of the nanocones shows three diffraction peaks, which is in good agreement with that of a JCPDS card (04-0850) and indicates the face-centered cubic (fcc) phase of Ni (Fig. S2a†).

Fig. 2b shows a top view of a SEM image of the MNN, which reveals a highly uniform coating of MnO_2 on the surface of NCAs. MnO_2 deposited on the plain Ni plate was prepared as the control sample (Fig. S1d†). The cross section image of MNN electrode shows that the thickness of the MNN is as thin as 3 μm which is thinner than most commercial Cu and Al foil (Fig. 2c). The MNN was peeled off from the Ti substrate and directly used as a supercapacitor electrode (photographic image in Fig. 1). The reduced thickness is advantageous for improving the volumetric energy density of the devices. Moreover, the simple preparation method renders it very suitable for large-scale manufacture (Fig. S19†).

The MNN film shows excellent mechanical robustness despite its small thickness. The tensile strength of the film is measured as high as 32.35 MPa, higher than those of commercial Cu foil (12 μm , 8.3 MPa) and Al foil (13 μm , 9.2 MPa). The data were calculated from the curves presented in Fig. S4.†

The MnO_2 -NCAs structures were further investigated by transmission electron microscopy (TEM). Fig. 2d distinctively manifests a uniform coating of MnO_2 on NCAs with an average thickness ~ 100 nm. The thickness of MnO_2 can be adjusted by the deposition time. Fig. 2e shows a magnified image of MnO_2 deposited on the surface of NCAs which gives a clear view of MnO_2 coating. It shows that the MnO_2 layer and NCAs have an excellent contact, which is benefited by the electro-deposition process at the surface. SAED from the area of MnO_2 is shown in the inset of Fig. 2f. However, the disperse rings and the weak diffraction peaks collectively indicate the poor crystallinity of as-prepared MnO_2 .

X-ray photoelectron spectroscopy (XPS) was used to determine the oxidation state of the as-prepared MnO_2 . Fig. S5b† shows a high resolution Mn 2p peak. The Mn 2p_{3/2} and Mn 2p_{1/2} peak are centered at 642.22 and 654.07 eV, respectively. The binding energy separation of the two peaks is 11.85 eV which is in good agreement with the reported value for MnO_2 .^{18,38} As shown in Fig. S5c,† the separation peak energies (ΔE_b) between the two Mn 3s component peaks can be used to identify the oxidation state of Mn in MnO_2 . The ΔE_b of 4.89 eV is between 4.8 and 5.3 eV for Mn^{4+} and Mn^{3+} , respectively.^{18,35} To further evaluate the specific valence of Mn in MnO_2 , we also analyzed the high resolution O 1s spectrum (Fig. S5d†).¹⁸ As a result of the analysis, the valence of Mn is 3.77 eV which coincides with the analysis of the Mn 3s spectrum.

As for the mechanical properties of MNN, we found that the MnO_2 nanostructures deposited on NCAs were robust enough to resist the peeling force of the scotch tape. To evaluate the cohesiveness of the MnO_2 layer on the current collector, a piece of scotch tape was attached to the surface of two electrode

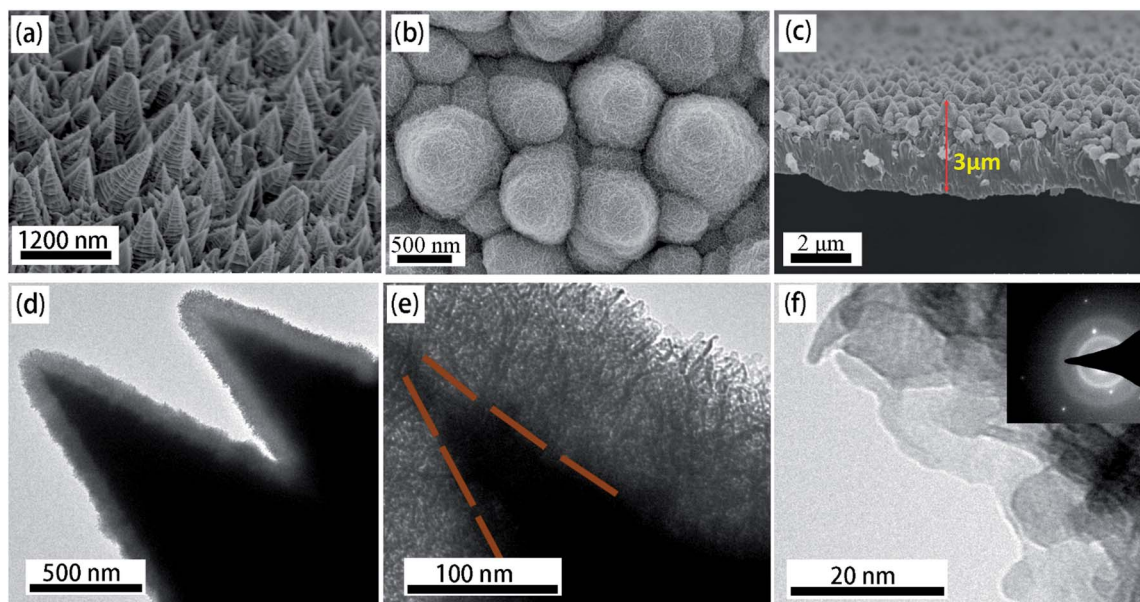


Fig. 2 (a) SEM image of NCAs. (b) SEM image of the MnO₂ nanostructure deposited on Ni nanocones. (c) Cross section of a MNN electrode. The electrode can be as thin as 3 μm. (d) TEM image of MNN. (e) Magnified TEM image of MNN. The partition lines outline the phase interface between Ni nanocone and the deposited MnO₂ nanostructure. (f) High-resolution (HR)-TEM image of MnO₂ deposited on the surface of a Ni nanocone. Inset is the selected area electron diffraction (SAED) pattern of MnO₂. It indicates the low crystallinity of MnO₂.

samples, one is the MNN film; and the other is the control sample of the MnO₂ deposited on a plain Ni plate (MNP) for comparison (Fig. S6a†). The scotch tape was peeled off after one minute. There was no obvious damage on the MNN surface; in contrast, some black powder from the MNP was transferred to the scotch tape and the underlying Ni plate became exposed (Fig. S6b†). The excellent cohesiveness of MNN could be attributed to the hierarchical structure where only a small area on the nanocone tip is in contact with the scotch tape, and the strong mechanical contact between MnO₂ and the rough Ni surfaces. Compared with the smooth surface of the Ni plate, the increased roughness of Ni nanocones is advantageous for the good adhesion between MnO₂ and the current collector. TEM analysis was used to investigate the MNN samples before and after the peeling test. Compared with the sample before the peeling test, the TEM image of MNN after the peeling test showed that the top of some nanocones became blunt slightly, which indicated a small amount of MnO₂ was possibly detached (Fig. S6c and d†). This observation suggests that the cone-like structure effectively contributes to the improved mechanical robustness.

CV was used to measure the capacitance of NCAs film, MNN and MNP electrodes by three-electrode configuration using 0.5 M Na₂SO₄ as the electrolyte (Fig. S7a†). No obvious capacitive behavior could be observed for NCAs. After the deposition of MnO₂, the CV curve of MNN becomes much larger and is close to an ideal rectangle shape, suggesting excellent supercapacitive characteristics.

Fig. 3a shows the CV curves of MNN at different scan rates. Even at a high scan rate of 1000 mV s⁻¹, the CV curve of MNN still shows a good rectangle shape, indicating an outstanding

rate performance (Fig. S7b†). The specific capacitance of MNN reached up to 632 F g⁻¹ at 2 mV s⁻¹, while it was only 244 F g⁻¹ for MNP. The dependence of the MNN specific capacitance on the scan rate is plotted in Fig. 3b, suggesting a larger specific capacitance than that of MNP. In terms of the areal specific capacitance, MNN and MNP are 31.6 and 12.2 mF cm⁻², respectively (Fig. S8†).

Fig. 3c and S9b† show the GCD curves of MNN and MNP, respectively. The GCD curve of MNN is nearly triangular, while MNP exhibits a large IR drop of 0.11 V at 5 A g⁻¹. The IR drop of MNP is due to the thicker MnO₂ layer at the same mass loading as compared with MNN and the weak adhesion between the MnO₂ and Ni plate. Nyquist plots of the electrochemical impedance spectroscopy (EIS) for MNN and MNP further confirmed this result (Fig. 3d). The intercept at real part of the high frequency represents a combined resistance of the ionic resistance of the electrolyte, the intrinsic resistance of the substrate and the contact resistance at the active material/current collector interface (R_e).³⁹ The charge-transfer resistance is caused by the Faradic reactions and the double-layer capacitance on the grain surface (R_{ct}).⁴⁰ Using a complex nonlinear least-squares (CNLS) fitting method for analysis,⁴¹ the R_e/R_{ct} of MNN is 6.267/2.023 Ω as compared with 6.928/17.220 Ω of MNP. The electrical equivalent circuit used for fitting impedance spectra is shown in Fig. S10.† The R_e and R_{ct} values of MNN electrode are both smaller than those of MNP. The improved EIS performance is related to higher adhesion between MnO₂ and Ni nanocone substrate, enhancement of the electrode surface and good porosity character of the MNN nanostructure, which provide an available transport channel and reduce the diffusion path.

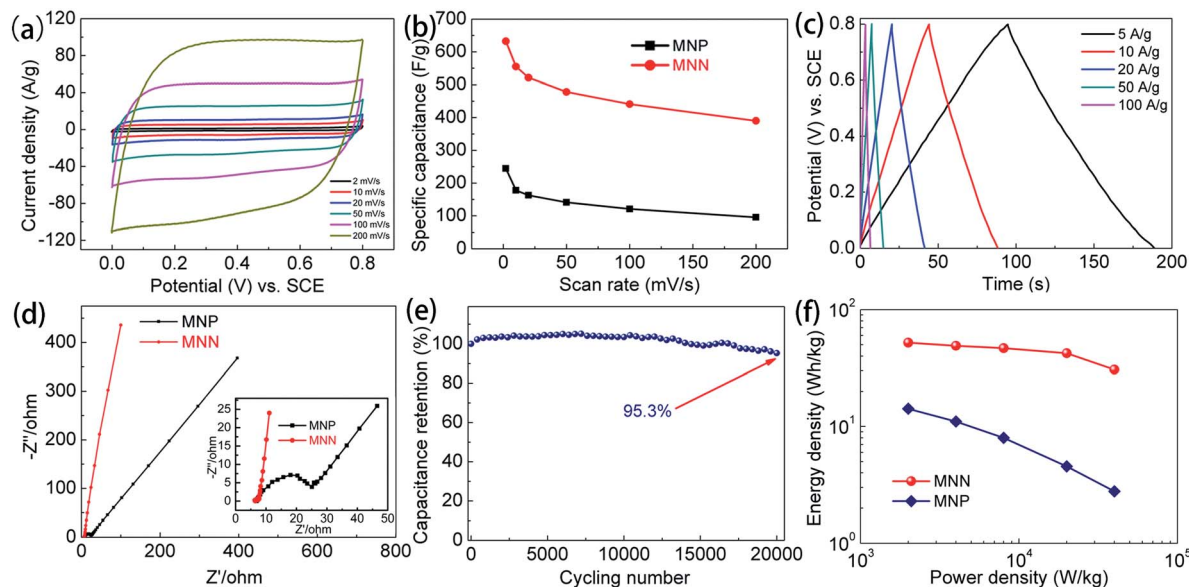


Fig. 3 (a) CV curves of the MNN electrode at different scan rates. (b) Specific capacitance of MNN and MNP as a function of the scan rates. (c) GCD curves of the MNN obtained at different current densities from 5 to 100 A g⁻¹. (d) Nyquist plots of the EIS for MNN and an MNP with a magnification of the high-frequency region is provided in the inset. (e) Capacitance retention of MNN as a function of the cycling number. The capacitance retention of MNN remains as high as 95.3% after 20 000 cycles. (f) Ragone plots of MNN and MNP.

In terms of energy density and power density of MNN and MNP, the highest energy of MNN reaches up to 52.2 W h kg⁻¹ at a power density of 2.0 kW kg⁻¹, while it is only 14.2 W h kg⁻¹ for MNP at a power density of 2.0 kW kg⁻¹ as shown in Fig. 3f. The energy density and power density are comparable to the results of MnO₂ nanopillars.²³ Unlike many other ever-reported transition metal oxide electrodes, the MNN electrode demonstrates ultrahigh cycling stability. As shown in Fig. S10,† even after 20 000 cycles at 50 mV s⁻¹, the CV curves still remain rectangular. The capacitance retention is as high as 95.3% after 20 000 cycles (Fig. 3e) which is higher than most reported MnO₂-based electrodes.^{19,23,42} The outstanding cycling performance is very important for the use of MnO₂-based supercapacitors in many applications. Additionally, the fabrication of NCAs can be scaled up by the as-designed roll-to-roll device, as shown in Fig. S19a.† A movie demonstrating the NCAs roll-to-roll process is provided in the ESI (Movie-2†).

Considering the results, the enhanced performance of MNN may be primarily attributed to four reasons: (1) the well-aligned Ni nanocones nanostructure increases the electrochemically active sites for the redox reaction; (2) the enlarged contact area between MnO₂ nanostructure and Ni nanocones substrates can shorten the electron transportation path length in the electrode; (3) the vertical Ni nanocones nanostructures increase the efficiency of electrolyte diffusion which leads to rate performance enhancement; (4) Ni has excellent mechanical properties (tensile strength and fracture toughness).

As compared to conventional water-based electrolytes, we selected ionic liquid as the electrolyte, since it provides a wider electrochemical window.⁴³ In order to fabricate all-solid-state supercapacitors, ionic liquid was mixed with some solid additives (polymer and silica, *etc.*) to form a gel-like electrolyte called

ionogel.³⁴ The ionogel allows a high voltage window (2.5 V) and easy shaping of the supercapacitor devices. The gel electrolyte was prepared by mixing EMIMBF₄ with FS nanopowder together (1 ml EMIMBF₄/400 mg FS) (Fig. S13†). The as-prepared all-solid-state supercapacitors are shown in Fig. S17† and the thickness was as small as 27 μm (PET film was applied to ensure good electrical contact). An aqueous-electrolyte supercapacitor prototype was fabricated for comparison.

Fig. 4a shows the CV curves of MNN/AC ionogel supercapacitors at different scan rates, which exhibit similar rectangular shapes. The Ragone plot of MNN/AC ionogel supercapacitor and MNN/AC aqueous supercapacitor is provided in Fig. 4c, and compares with commercially available energy storage systems including as-prepared aqueous supercapacitor, commercial AC/AC supercapacitor, LSG supercapacitors (aqueous electrolyte and ionogel electrolyte), 3 V/300 μF aluminum electrolytic capacitors and 500 μA h lithium thin-film battery.²⁴ The energy and power densities of MNN/AC ionogel supercapacitors and aqueous supercapacitor were calculated by eqn (3). And the data were from Fig. 4b and S16a.† Vol refers to the total volume of the supercapacitor, including the PET package. Apparently, the energy density of our ionogel-based supercapacitor is higher than that of an aqueous supercapacitor due to the larger potential window of the ionogel supercapacitor. It can reach a higher energy density when compared with an AC/AC supercapacitor as a result of the use of transition metal oxide and scaling down of the electrode dimensions to the micro-scale. It can reach as high as 2.7 × 10⁻³ W h cm⁻³ at a power density of 3.5 × 10⁻³ W cm⁻³. The energy density is about 40 times and 2300 times that of a LSG supercapacitor (aqueous electrolyte) and aluminum electrolytic capacitor, respectively. What is more, the energy density is

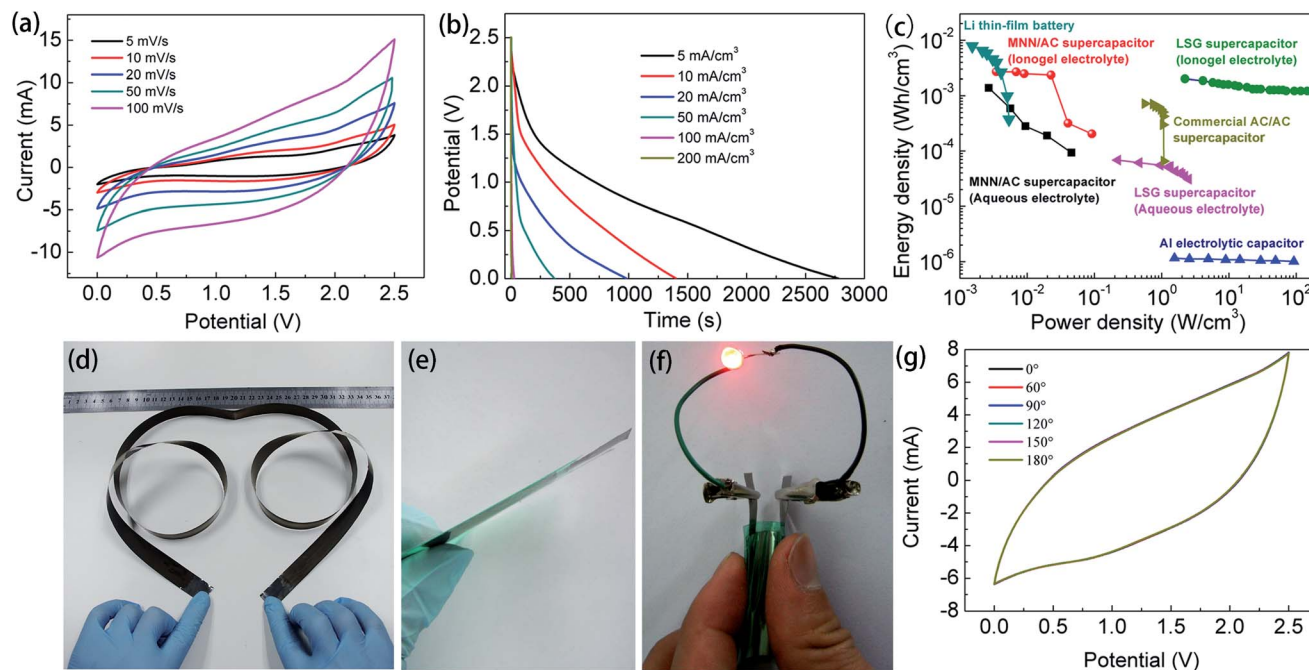


Fig. 4 (a) CV curves of a MNN/AC ionogel supercapacitor at different scan rates from 5 to 100 mV s^{-1} . (b) Discharged curves of MNN/AC ionogel supercapacitor at different current densities. (c) Energy and power densities of the MNN-based asymmetric supercapacitors compared to some available energy storage systems. (d) A photographic image of the as-prepared MNN/AC ionogel supercapacitor electrode (1.3 m) obtained from a roll-to-roll preparation instrument. (e) Photographic image of a fully packed supercapacitor device (PET films were applied to ensure good electrical contact). (f) Photograph showing a MNN/AC ionogel supercapacitor driving a red LED (1.8 V, 20 mA) under a bending state. (g) CV curves of an asymmetric supercapacitor under different bending angles at 50 mV s^{-1} . There is no obvious change of the CV curves indicating the outstanding flexibility of an ionogel supercapacitor.

higher than the recently reported ionogel based LSG supercapacitor.

The charged energy storage devices, including charged batteries and supercapacitors, are in a state of high free energy relative to that of the discharged state, leading to a thermodynamic driving force for them to self-discharge.⁴¹ During the process of self-discharge, the voltage decay of a charged supercapacitor was caused by a small amount of leakage current. In order to measure the self-discharge behaviour of the supercapacitors, the devices were charged to V_{max} . The asymmetric supercapacitors based on 0.5 M Na_2SO_4 aqueous electrolyte and ionic liquid gel electrolyte were charged to 2.0 and 2.5 V, respectively (Fig. S15†). They took more than 8 h to drop to approximately 0.9 and 1.0 V, respectively. The results are better than some reported carbon-based supercapacitors.^{44,45} The excellent performance for the nanocones-based supercapacitors demonstrates a promise for practical applications.

The ultrathin supercapacitor can be seen from Fig. 4e. In order to further demonstrate the practical usage of the ultrathin micro-supercapacitor, we connected two supercapacitor units in series and in parallel to create tandem devices. The as-fabricated tandem cells exhibit excellent control over the operating voltage window and capacitance. Fig. S18a† shows an extended potential from 2.5 V for a single device to 5.0 V for two devices connected in series. Meanwhile, the tandem cell (connected in parallel) exhibits twice the charge/discharge time under the same potential window as compared with the single

supercapacitor unit (Fig. S18b†). The performance of the tandem cell indicates a high value of ultrathin supercapacitors for practical applications.

The as-prepared ionogel supercapacitor was used to drive a red LED (1.8 V, 20 mA) under a bending state, as shown in Fig. 4f. CV tests were carried under different bending angles which revealed negligible changes. Similarly, the supercapacitor lit up a red LED without obvious brightness dimming during the repeated bending process (ESI, Movie-1†). The above evidence convincingly demonstrates the remarkable flexibility of an as-prepared ultrathin supercapacitor. A cycling test was also applied to the flexible ionogel supercapacitor. After cycling for 5000 cycles, the supercapacitor device demonstrated less than 9% capacitance reduction, indicating an excellent cycling performance (Fig. S14†).

Conclusions and outlook

In summary, we report the deposition of MnO_2 onto the highly ordered NCAs film which can be easily peeled off from the Ti substrate for free-standing Ni nanocones supported ultrathin electrodes (as thin as 3 μm). This unique electrode structure enables a high specific capacitance (632 F g^{-1}), outstanding cycle performance (20 000 cycles with 4.7% loss) and excellent energy density (52.2 W h kg^{-1}). The tensile strength of the electrode thin film is higher than those of commercial Cu and Al foils. Compared with conventional methods, the fabrication of

the electrodes can be scaled up easily by applying a roll-to-roll device. All-solid-state asymmetrical micro-supercapacitors (27 μm in thickness) with enhanced energy density (as high as $2.7 \times 10^{-3} \text{ Wh cm}^{-3}$) are fabricated based on the ultrathin electrodes. Excellent mechanical performance, flexibility and electrochemical stability of the devices were demonstrated. Given the outstanding performance characteristics, we look forward to a vast application of these flexible micro-supercapacitors as a power source for wearable electronics and other miniaturized applications, especially in cases which need winding, folding, twisting, and even laminating the device. As a general one, our technique is applicable to a large range of material species besides MnO_2 . We envisage it would arouse interest to a wide range of promising applications.

Acknowledgements

This work is financially supported by the Shenzhen Peacock Plan no. KQCX20120814155245647, the Shenzhen Technical Project no. JCYJ20130402145002411, and the National Nature Science Foundation of China no. 51202120.

References

- 1 M. Beidaghi and Y. Gogotsi, *Energy Environ. Sci.*, 2014, **7**, 867–884.
- 2 M. F. El-Kady and R. B. Kaner, *Nat. Commun.*, 2013, **4**, 1475–1483.
- 3 D. Pech, M. Brunet, H. Durou, P. Huang, V. Mochalin, Y. Gogotsi, P.-L. Taberna and P. Simon, *Nat. Nanotechnol.*, 2010, **5**, 651–654.
- 4 M. F. El-Kady, V. Strong, S. Dubin and R. B. Kaner, *Science*, 2012, **335**, 1326–1330.
- 5 Z. Cai, L. Li, J. Ren, L. Qiu, H. Lin and H. Peng, *J. Mater. Chem. A*, 2013, **1**, 258–261.
- 6 B. E. Conway, *J. Electrochem. Soc.*, 1991, **138**, 1539–1548.
- 7 C.-C. Hu, K.-H. Chang, M.-C. Lin and Y.-T. Wu, *Nano Lett.*, 2006, **6**, 2690–2695.
- 8 S. Chen, J. Zhu, X. Wu, Q. Han and X. Wang, *ACS Nano*, 2010, **4**, 2822–2830.
- 9 Z. Su, C. Yang, C. Xu, H. Wu, Z. Zhang, T. Liu, C. Zhang, Q. Yang, B. Li and F. Kang, *J. Mater. Chem. A*, 2013, **1**, 12432–12440.
- 10 P. Yang, Y. Ding, Z. Lin, Z. Chen, Y. Li, P. Qiang, M. Ebrahimi, W. Mai, C. P. Wong and Z. L. Wang, *Nano Lett.*, 2014, **14**, 731–736.
- 11 X.-h. Xia, J.-P. Tu, Y.-J. Mai, X.-L. Wang, C.-D. Gu and X.-B. Zhao, *J. Mater. Chem.*, 2011, **21**, 9319–9325.
- 12 D.-H. Ha, L. M. Moreau, S. Honrao, R. G. Hennig and R. D. Robinson, *J. Phys. Chem. C*, 2013, **117**, 14303–14312.
- 13 C. Yuan, X. Zhang, L. Su, B. Gao and L. Shen, *J. Mater. Chem.*, 2009, **19**, 5772–5777.
- 14 J. Jiang, Y. Li, J. Liu, X. Huang, C. Yuan and X. W. D. Lou, *Adv. Mater.*, 2012, **24**, 5166–5180.
- 15 M. Zhi, C. Xiang, J. Li, M. Li and N. Wu, *Nanoscale*, 2013, **5**, 72–88.
- 16 C.-C. Hu and C.-C. Wang, *J. Electrochem. Soc.*, 2003, **150**, A1079–A1084.
- 17 C. Lokhande, D. Dubal and O.-S. Joo, *Curr. Appl. Phys.*, 2011, **11**, 255–270.
- 18 M. Toupin, T. Brousse and D. Bélanger, *Chem. Mater.*, 2004, **16**, 3184–3190.
- 19 G. Yu, L. Hu, N. Liu, H. Wang, M. Vosgueritchian, Y. Yang, Y. Cui and Z. Bao, *Nano Lett.*, 2011, **11**, 4438–4442.
- 20 X. Lu, T. Zhai, X. Zhang, Y. Shen, L. Yuan, B. Hu, L. Gong, J. Chen, Y. Gao and J. Zhou, *Adv. Mater.*, 2012, **24**, 938–944.
- 21 C. Choi, J. A. Lee, A. Y. Choi, Y. T. Kim, X. Lepró, M. D. Lima, R. H. Baughman and S. J. Kim, *Adv. Mater.*, 2013, **26**, 2059–2065.
- 22 P. Simon and Y. Gogotsi, *Nat. Mater.*, 2008, **7**, 845–854.
- 23 Z. Yu, B. Duong, D. Abbitt and J. Thomas, *Adv. Mater.*, 2013, **25**, 3302–3306.
- 24 W. Chen, R. Rakhi, L. Hu, X. Xie, Y. Cui and H. Alshareef, *Nano Lett.*, 2011, **11**, 5165–5172.
- 25 W. Geng, A. Hu and M. Li, *Appl. Surf. Sci.*, 2012, **263**, 821–824.
- 26 T. Hang, H. Ling, A. Hu and M. Li, *J. Electrochem. Soc.*, 2010, **157**, D624–D627.
- 27 S. Zhang, Z. Du, R. Lin, T. Jiang, G. Liu, X. Wu and D. Weng, *Adv. Mater.*, 2010, **22**, 5378–5382.
- 28 T. Y. Wei, C. H. Chen, H. C. Chien, S. Y. Lu and C. C. Hu, *Adv. Mater.*, 2010, **22**, 347–351.
- 29 J. W. Lee, A. S. Hall, J.-D. Kim and T. E. Mallouk, *Chem. Mater.*, 2012, **24**, 1158–1164.
- 30 Z.-D. Huang, B. Zhang, R. Liang, Q.-B. Zheng, S. W. Oh, X.-Y. Lin, N. Yousefi and J.-K. Kim, *Carbon*, 2012, **50**, 4239–4251.
- 31 M. Sukácho, *J. Mater. Chem.*, 2011, **21**, 18215–18219.
- 32 G. Yu, L. Hu, M. Vosgueritchian, H. Wang, X. Xie, J. R. McDonough, X. Cui, Y. Cui and Z. Bao, *Nano Lett.*, 2011, **11**, 2905–2911.
- 33 Y. He, W. Chen, X. Li, Z. Zhang, J. Fu, C. Zhao and E. Xie, *ACS Nano*, 2012, **7**, 174–182.
- 34 J. Le Bideau, L. Viau and A. Vioux, *Chem. Soc. Rev.*, 2011, **40**, 907–925.
- 35 J.-G. Wang, Y. Yang, Z.-H. Huang and F. Kang, *J. Mater. Chem.*, 2012, **22**, 16943–16949.
- 36 Z. Lei, Z. Liu, H. Wang, X. Sun, L. Lu and X. Zhao, *J. Mater. Chem. A*, 2013, **1**, 2313–2321.
- 37 X. Yang, F. Zhang, L. Zhang, T. Zhang, Y. Huang and Y. Chen, *Adv. Funct. Mater.*, 2013, **23**, 3353–3360.
- 38 S. W. Lee, J. Kim, S. Chen, P. T. Hammond and Y. Shao-Horn, *ACS Nano*, 2010, **4**, 3889–3896.
- 39 J. Gamby, P. Taberna, P. Simon, J. Fauvarque and M. Chesneau, *J. Power Sources*, 2001, **101**, 109–116.
- 40 Z. Fan, J. Yan, T. Wei, L. Zhi, G. Ning, T. Li and F. Wei, *Adv. Funct. Mater.*, 2011, **21**, 2366–2375.
- 41 B. Conway, *Electrochemical supercapacitors: scientific fundamentals and technological applications (POD)*, Kluwer Academic/Plenum, New York, 1999.
- 42 Z. Li, Y. Mi, X. Liu, S. Liu, S. Yang and J. Wang, *J. Mater. Chem.*, 2011, **21**, 14706–14711.
- 43 J. F. Wishart, *Energy Environ. Sci.*, 2009, **2**, 956–961.
- 44 Q. Zhang, J. Rong, D. Ma and B. Wei, *Energy Environ. Sci.*, 2011, **4**, 2152–2159.
- 45 L. Yuan, X.-H. Lu, X. Xiao, T. Zhai, J. Dai, F. Zhang, B. Hu, X. Wang, L. Gong and J. Chen, *ACS Nano*, 2011, **6**, 656–661.